Classification of Pain Intensity using Functional Connectivity Networks Derived from Intracranial Electroencephalography in Humans

Timmy Pham

A thesis

submitted in partial fulfillment of the

requirements for the degree of

Master of Science

University of Washington

2023

Committee:

Rajesh P. N. Rao

Jeffrey G. Ojemann

Azadeh Yazdan

Program Authorized to Offer Degree:

Bioengineering

University of Washington

Abstract

Classification of Pain Intensity using Functional Connectivity Networks Derived from Intracranial Electroencephalography in Humans

Timmy Pham

Chair of the Supervisory Committee:
Rajesh P. N. Rao
Paul G. Allen School of Computer Science

Pain is an innate response most commonly arising from sensory and emotional stimuli reflecting injury or illness. Brain structures such as the anterior cingulate cortex, insula, and thalamus have been previously implicated in neural pain networks. However, the strength and nature of the relationships between pain structures have yet to be fully characterized. Intracranial electroencephalography (iEEG) is a method to record neural electrophysiology from cortical and subcortical regions of the brain, and its high spatial and temporal resolution has been used to identify neurophysiological networks associated with various conditions and cognitive states. Here, we collected pain reports using the 0 to 10 clinical visual analog scale and recorded multi-day iEEG in patients undergoing clinical seizure monitoring (n=5). For each pain report, 5-minute windows of iEEG from more than 87 channels were extracted, and neural features such as total power-in-band, correlation, and coherence were calculated and used as inputs in subject-specific pain classification models. Across subjects, multi-channel logistic regression models had a 76 $\pm$ 9% accuracy in classifying binarized pain states (low vs. high pain) and multi-channel random forest models had 64 $\pm$ 21% accuracy in classifying discrete VAS scores (0–10). The best-performing model had a 95% classification accuracy of discrete VAS scores. Our results indicate that subject-specific pain networks can be constructed from multi-day iEEG and be used to predict reported pain intensities. The machine learning paradigm described here can help inform closed-loop neuromodulation and pharmacological approaches for treating pain.

INTRODUCTION

Pain, a multidimensional sensory and emotional experience, is commonly experienced postoperatively, with approximately 75% of patients reporting medium to severe acute pain following surgery [1]. Acute pain that persists beyond the typical recovery period of an injury or operation can transition into chronic pain, a condition affecting more than 20% of the global adult population and the leading cause of disease and disability burden [2]–[4]. Unfortunately, there is no universal treatment for pain due to its high subjectivity and variation across type of stimuli and an individual's mood, attention, memory, and more [5]. Common acute pain management strategies involve the prescription of pain medicines such as opioids, which while highly effective, increase the risk of misuse and addiction [6], [7]. Behavioral practices such as therapy, hypnosis, and yoga may also be effective but are not suitable for all subjects [8]. Neuromodulation techniques, such as deep brain stimulation, have been shown to be highly effective in subjects where the sources of pain were known and stimulation in those areas was feasible [9]. Unfortunately, source localization and stimulation technologies remain expensive and invasive [10], [11]. Fundamentally, pain relief is constrained by two factors: insufficient mechanistic explanations and inadequate tools for assessing an individual's experience of pain.

Traditional models of pain outline pathways that terminate in various circuits of the brain [12]–[14]. Generally, pain is understood to arise along the nociceptive or neuropathic pain pathways. In the nociceptive pain pathway, noxious stimuli induce peripheral sensitization in the nociceptors, increasing action potential firing and signal transmission in the dorsal horn of the spinal cord. The dorsal horn neurons induce central sensitization, a cascade of biochemical reactions that work to transmit nociceptive information to the thalamus of the brain where the central processing of pain signals occurs. In contrast, neuropathic pain involves the direct injury to nerves in the peripheral or central nervous system. In a similar manner to nociceptive pain, neuropathic pain induces central sensitization in response to stimulus-independent activity and direct damage to nerve fibers.

Following central sensitization, pain signals received by the thalamus are believed to flow to other regions of the cerebral cortex, inducing unique responses based on concurrent emotional and environmental states [12]. Neuroimaging has highlighted the interconnectedness of pain structures in what is known as the pain matrix [15]. These structures are postulated to exist in regions involving the primary somatosensory cortex, secondary somatosensory cortex, anterior cingulate cortex, prefrontal cortex, insular cortex, amygdala, thalamus, cerebellum, and periaqueductal gray matter. It is further hypothesized that within the pain matrix, the lateral pain pathway is correlated with sensory aspects of pain and the medial pain pathway is associated with emotional aspects [16]. Other approaches to identifying pain circuitry have analyzed lesions in the brain. For example, Recent investigations using neural electrophysiology data gathered from electroencephalography, electrocorticography, and magnetoencephalography have demonstrated the promise of analyzing neural activity for the characterization of pain under various stimuli [17]. Where imaging methods provide critical spatial information, electrophysiological methods provide temporal information that can capture neural events as they unfold.

Neural events can be fluctuations in electric potential across regions of the brain that are thought to be the result of active cellular processes, such as synaptic activity, which reflect signal transmission to and from other regions [18]. Functional connectivity analysis involves methods for assessing neural activity and can be applied to both neuroimaging and electrophysiology to

derive insights about neurological disorders, cognitive states, and behaviors [19]. For example, networks constructed from functional connectivity analysis have been able to distinguish between subjects with Alzheimer's disease and those with healthy aging, as well as between depressed subjects and healthy subjects [20], [21]. Other classifications have been made using functional connectivity analysis in regards to epilepsy, memory, and multiple sclerosis [22]–[24]. For pain assessment, functional connectivity analysis has been applied in fMRI data to differentiate between varying intensities of heat-induced pain in a non-clinical setting [25].

Here, we develop a machine learning paradigm for classifying subject-specific pain states from post-surgical fluctuations in pain using single-site and functional connectivity analysis on intracranial electroencephalography. Our subject dataset comprises subjects with drug-resistant epilepsy undergoing seizure monitoring who experience varying pain over their 7–10 day stay in the hospital. The intensity of a subject's pain was recorded at unscheduled intervals using the visual analog scale (VAS), reported numerically from 0–10. We time-synchronized the subject's neural activity to these pain reports and extracted both temporal and spectral features, such as Spearman's correlation, total power-in-band (PIB), and coherence. These features were then used to construct and implement in pain networks at three levels: single-channel, dual-channel, and multi-channel **(Figure 1)**. Using generalized linear models (GLM), classification and regression tree (CART), and ensemble methods, we aim to identify pain networks that can classify subject-specific pain intensity. The identification of suitable pain networks advances investigations into neural mechanisms of pain on two fronts by (1) identifying electrophysiological relationships involved in pain processing and (2) demonstrating pain profiles that can highlight unique, subject-specific responses to pain for use in informing neuromodulation methods and other pain management strategies.

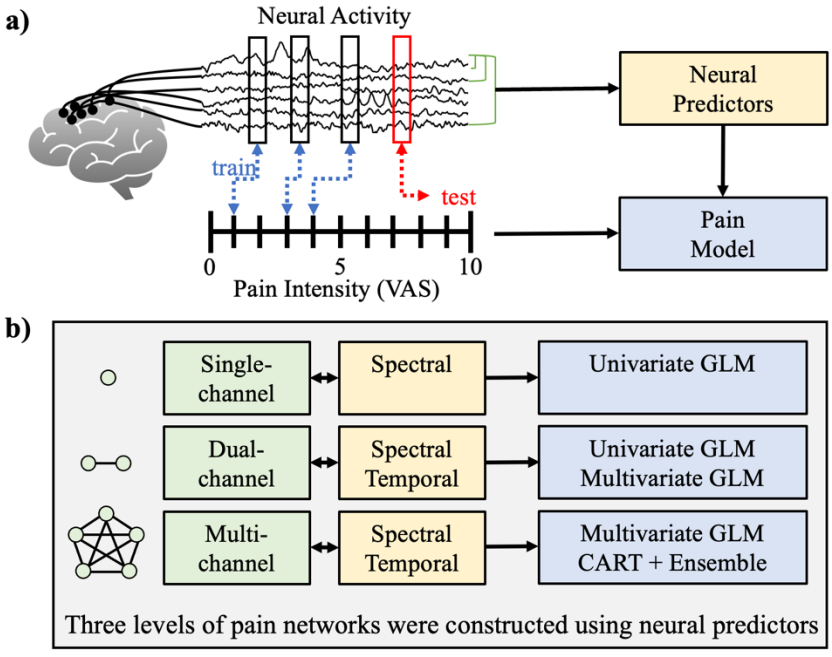

Fig. 1. Neural decoding paradigm. a) Windows of neural activity are time-synchronized with subject pain reports at varying intensities recorded with the visual analog scale (VAS). Neural predictors are extracted from the windows of activity and used as inputs to pain prediction models. b) Single-channel, dual-channel, and multi-channel models were investigated by

combining neural activity time-series. Models increased in complexity with the addition of channels and feature types.

METHODS

Neural Data Acquisition

Intracranial electroencephalography (iEEG) electrodes were implanted in subjects with intractable epilepsy (n=5) at Harborview Medical Center (HMC) for seizure monitoring and the identification of epileptogenic zones. Data collection was facilitated in conjunction with the EEG and Neurophysiology Laboratory at HMC. All experiments were approved by the University of Washington Institutional Review Board. Informed consent was obtained for all subjects.

Neural electrophysiology data was recorded using either implanted stereo-electroencephalography (sEEG) electrodes or subdural multi-contact electrocorticography (ECoG) grids. sEEG electrodes (PMT Corp, USA) range from 8 to 16 individual recording channels per electrode and have a 0.8 mm diameter with 3.5 mm spacing. ECoG grids (Ad-Tech, USA) consist of 8-64 individual recording channels and have a 2.3 mm diameter with 10 mm spacing between contacts. Electrode implant locations were clinically determined, resulting in varying electrode coverage across subjects (**Figure 2**). Neural electrophysiology was sampled at 500 Hz in up to 256 total electrodes over 5–7 days.

Data was preprocessed with a notch filter to remove line noise at 60 Hz and its harmonics at 120 Hz and 180 Hz. Since local field potential activity typically lies within the 0.1–200 Hz range, a 200 Hz 5th-order Butterworth low-pass filter was applied to remove high frequency activity. Preprocessed data was visualized for quality and identification of potentially unusable recording channels due to excessive noise or artifacts.

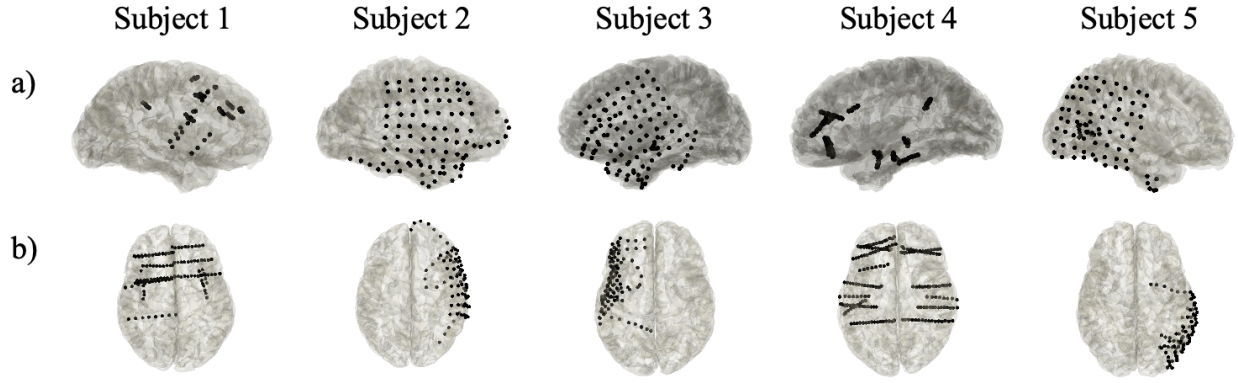

Figure 2. Subject channel coverage in a) sagittal view and b) axial view. Subjects 2, 3, and 5 have surface ECoG electrodes concentrated in one hemisphere, and Subjects 1 and 4 have bilateral sEEG.

Pain Intensity Reports

Subjects were asked to report their pain intensity based on the visual analog scale (VAS) throughout their stay in the hospital. The VAS is widely used as a means of measuring pain and consists of an interpretable horizontal line representing different pain intensities from left to right, 0 being no pain and 10 being the worst pain imaginable [26]. The time of VAS reporting, pain intensities, pain descriptors (mild, moderate, and severe), location of pain, and pain patterns (none,

intermittent, and continuous) were recorded. VAS scores were recorded several times a day as part of routine clinical care over the duration of the subject's stay. In our subjects, we recorded a range of 27-60 VAS scores (**Table 1**).

In our binary classification task, we further defined subject-specific "low" and "high" pain states by using the median intensity of the subject's VAS distribution as the dividing threshold. In practice, these thresholds can be defined by an appropriate clinical assessment.

Feature Extraction

Our five subjects had between 87-200 iEEG implanted electrodes and a range of 27-60 pain intensities recorded **(Table 1)**.

Table 1. Subject Profiles

Subject	Age	Sex	Channels	VAS Scores	Type
1	24	F	129	27	sEEG, bilateral
2	33	F	93	37	ECoG, right hemisphere
3	43	M	113	56	ECoG, left hemisphere
4	32	M	200	37	sEEG, bilateral
5	20	M	87	60	ECoG, right hemisphere

Windows of neural activity surrounding each instance of VAS reporting were extracted and subsequently used for pain state classification. We defined a total window size of 5 minutes, which comprised the 2 and a half minutes before and after the VAS was collected. We made an assumption that the subject's pain did not significantly change during this 5-minute window. Each neural window was further divided into 10, 30-second epochs.

In single-channel models, we computed the total power-in-band for each of the canonical frequency bands: delta (0.1–4 Hz), theta (4–8 Hz), alpha (8–12 Hz), beta (12–30 Hz), gamma (30–55 Hz), and high gamma (65–200 Hz). To compute the total power in each band, we applied a 2nd order Butterworth filter with the cutoff frequencies specified above and a Hilbert transformation to obtain its analytical signal, which was subsequently squared and summed across the epoch to obtain the total power-in-band.

In multi-channel models, we further computed connectivity measures between channels, including Spearman's correlation coefficient and coherence across all bands. These connectivity measures were selected to capture behaviors associated with inter-channel oscillatory similarities, both in the time domain with correlation metrics and in the frequency domain with coherence [19].

Single-channel Pain Classification

For each channel, a univariate logistic regression model using Scikit-learn (Python v. 3.9) was fit to map the relationship between the total power-in-band estimates and the binarized subject-reported pain intensities [27]. We fit the model on 70% of the data and tested on the other 30%. Model accuracy was computed individually across all combinations of single-channel and

frequency band. We also evaluated single-channel classification performance of the discrete VAS scores, in contrast to the binarized VAS scores, using linear discriminant analysis.

Bottom-up Network Construction and Multi-channel Pain Classification

We selected the 10 channels with the highest model performance from the single-channel logistic regression models as pain network candidates. Pain networks were constructed by assessing connectivity measures between all channel pairs. Spearman's correlation coefficient yielded

$$n_{channels}(n_{channels} - 1)/2$$

additional features, and coherence calculations included

$$n_{bands} * n_{channels}(n_{channels} - 1)/2$$

features to represent each of the canonical frequency bands. In total, these connectivity measures constituted *k* additional features, where

$$k = (1 + n_{bands}) * n_{channels}(n_{channels} - 1)/2.$$

The data was divided into 70% training data and 30% testing data. In multi-channel binary classification, random forest, decision tree, and multivariate logistic regression models were constructed using Scikit-learn (Python v. 3.9) [27]. In addition to binary classification, these same models, excluding logistic regression, were used in predicting discrete VAS scores. Additionally, linear regression and random forest regression models were trained and evaluated against a continuous 0 to 10 scale. Feature importance was evaluated by computing the Gini impurity in the decision tree and ensemble models [28].

Top-down Network Construction

Lastly, we constructed pain networks by computing connectivity metrics across all possible channel pairs. First, we binarized the VAS scores and separately averaged connectivity measures (e.g., Spearman's correlation coefficient) for channel pairs in the "low pain state" and the "high pain state." Pain networks were constructed via thresholding of the connectivity values, where increasing the threshold reduced the number of network connections. Furthermore, a differential pain network was constructed by thresholding the difference between the connectivity values of the high pain state and the low pain state to yield approximately 10 channels. Finally, the channels selected from the top-down network construction were compared to the bottom-up network construction.

RESULTS

Across all 5 subjects, a total of 217 pain intensities were clinically recorded, with an average recorded intensity of 4.3 $\pm$ 2.5 and an average within-subject range of 7.2 $\pm$ 2.4. Not all subjects reported pain intensities that span the entire VAS (0-10) scale. Additionally, subject electrode coverage varied in location, type, and duration of recording. Due to these differences and the anticipated subjectivity of pain, we developed subject-specific models for pain prediction.

Single-channel Pain Prediction

We first assessed the prediction performance of single-channel models **(Figure 3)**. Logistic regression models were trained using total power-in-band (PIB) values to predict binary pain states (low vs. high). Every combination of recording channel and canonical frequency band (delta, theta, alpha, beta, gamma, and high gamma) constituted a unique instance of the model. For example, in subject 1, there were 774 logistic regression models, representing 129 channels by 6 frequency bands. The maximum prediction accuracy across all subjects was 99.1%, trained used PIB values from the beta band of the inferior frontal gyrus pars opercularis of Subject 2. We applied a benchmark null comparison of the best performing model by randomizing the labels and as expected in a binary classification problem with roughly equal labels, the logistic regression model accuracy was 50.5%. All subjects had a maximum prediction accuracy greater than 68%, with subject-specific averages ranging from 54.9–64.8%.

Next, we trained linear regression models to predict continuous pain intensity using the same PIB values. The best performing model had an R^2 of 0.71 and was trained using PIB values from the high-gamma band of the middle frontal gyrus of Subject 2. In most instances, the linear regression model performed poorly, with most models having $R^2 < 0.20$ across subject.

Classification of discrete VAS scores was performed using linear discriminant analysis (LDA) models trained on the PIB values. The best performing LDA model was again in Subject 2 at 77%, trained using PIB values from the beta band of the temporal pole. Subject 5 had the lowest maximum classification accuracy at 26%, with the model trained using PIB values from the delta band of the middle temporal gyrus. For reference, a null model in each subject is expected to yield a prediction accuracy of

$$\frac{1}{|\{intensities\}|}$$

where $|\{\text{intensities}\}|$ represents the unique number of intensities reported for a given subject assuming uniform classes. The VAS distribution was not uniform for each patient, and the null test for Subject 2 provided a reference classification of 56% (see **Discussion**).

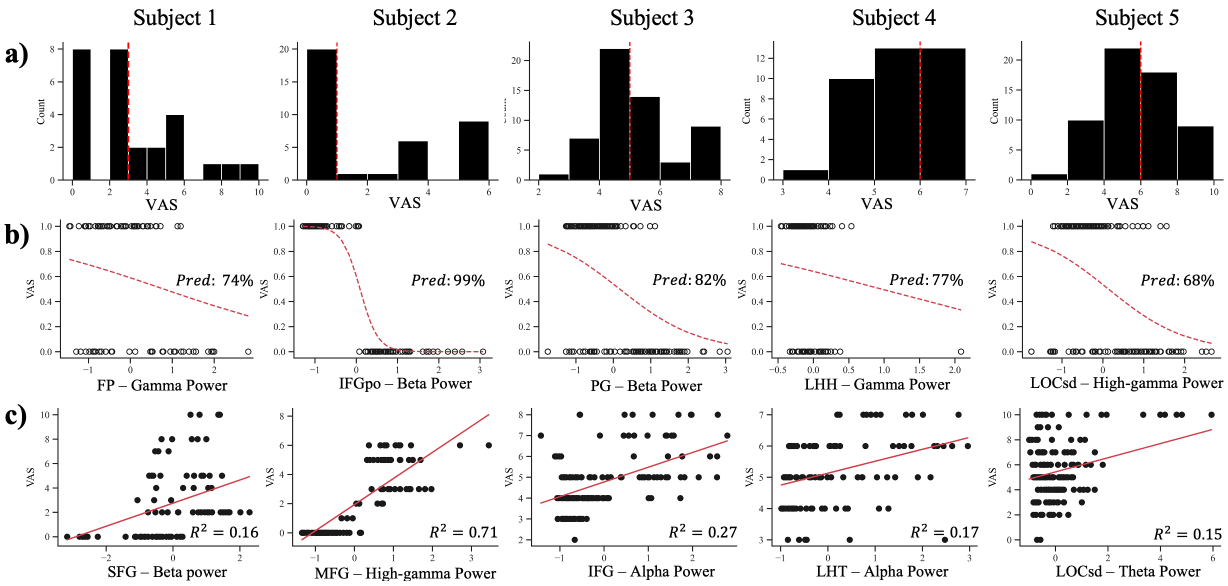

Fig. 3. Pain prediction models trained on total power-in-band (PIB) in individual channels. a) Reported visual analog scale (VAS) pain distributions. b) Best performing logistic regression model trained using normalized total PIB values across pain reports. c) Best performing linear regression model trained using normalized total PIB values across pain reports. *FP – frontal pole; IFGpo – inferior frontal gyrus pars opercularis; LHH – left hippocampal head; LOCsd – lateral occipital cortex superior division; SFG – superior frontal gyrus, MFG – middle frontal gyrus; IFG – inferior frontal gyrus; LHT – left hippocampal tail.*

Dual-channel Pain Prediction

We constructed pain networks using the top 10 channels from the highest performing logistic regression models (**Table 2**). We constrained network size to 10 channels to reduce computational complexity as would be required in real-time pain decoding. These channels were recruited from all regions at all frequency ranges. Across subjects, 21 of the 50 top-performing models utilized PIB values from the gamma or high-gamma bands (see **Supplementary Table 1**). PIB values from the beta-band were involved in 12 of the 50 models. Delta PIBs only presented in 2 of the models.

Table 2. Bottom-up Network Construction

Subject	Type	Top 10 Channels
1	sEEG, bilateral	**Middle frontal gyrus** (n=2), **frontal pole** (n=2), **cingulate gyrus** (n=2), **postcentral gyrus** (n=2), **precentral gyrus** (n=1), **paracingulate gyrus** (n=1)
2	ECoG, right hemisphere	**Inferior frontal gyrus** (n=2), **temporal pole** (n=2), **precentral** gyrus (n=2), **middle frontal gyrus** (n=1), **supramarginal gyrus** (n=1), **central opercular cortex** (n=1), **frontal orbital cortex** (n=1)
3	ECoG, left hemisphere	**Middle frontal gyrus** (n=4), **inferior frontal gyrus** (n=3), **superior temporal gyrus** (n=2), **precentral gyrus** (n=1)
4[1]	sEEG, bilateral	**Hippocampus** (n=3), **anterior cingulate cortex** (n=2), **amygdala** (n=2), **occipital frontal** (n=2), **posterior cingulate cortex** (n=1)
5	ECoG, right hemisphere	**Occipital cortex** (n=5), **inferior temporal gyrus** (n=2), **angular gyrus** (n=2), **supramarginal gyrus** (n=1)

From these pain networks, we evaluated connectivity metrics of each channel pair for prediction performance of both binary pain states and the discrete VAS scale **(Figure 4)**. Spearman's correlation coefficient was computed between channel pairs for every pain report and used to train binary logistic regression and linear regression models. In binary decoding, correlations within the precentral gyrus had the highest prediction accuracy of pain intensities at 76% in Subject 2. The lowest binary decoding performance was in Subject 5, with a performance of 54%. With linear regression, Subject 2 correlations between the inferior frontal gyrus and precentral gyrus had the highest association with pain intensities, with an R^2 of 0.46. Spearman's correlations had a poor association with pain intensities in Subject 5, having a maximum R^2 of 0.04.

[1] ECGL, an electrocardiogram signal was initially included in the top 10 performing channels as it demonstrated a binary classification accuracy of 75.7%. ECG signals have been previously used in attempts to decode acute pain [29]. For the purposes of network construction, the next top-performing channel was selected in place of ECGL to better model neural dynamics.

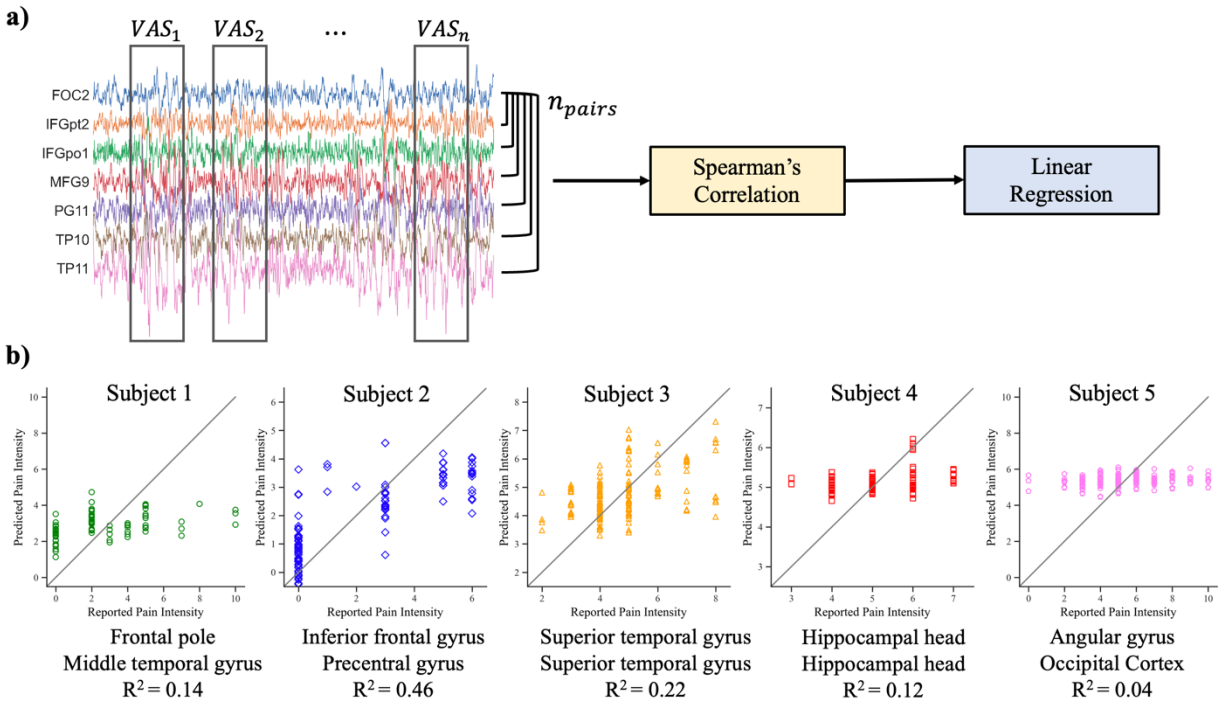

Fig. 4. Pain prediction models trained on Spearman's rank correlation coefficient between the top 10 channel pairs. a) Correlations are computed for every channel pair across all reported pain intensities (VAS). b) Best performing linear regression model in each subject using channel pair correlations. Channel connections and R^2 values for the best performing models are reported. Ideal pain prediction shown in gray.

Multi-channel Pain Prediction

Next, we trained classifiers using features extracted from the 10-channel pain network, including Spearman's correlation coefficient and coherences between channel pairs, as well as individual PIBs **(Figure 5).** Model performances were assessed in predicting both binary pain states **(Table 3)** and the discrete VAS scale **(Table 4)**. The best performing model in both assessments was random forest, with a binary prediction average of 80% and discrete VAS prediction average of 65% across all subjects. Evaluating the testing dataset with an error tolerance of $\pm$ 1 VAS provided for a discrete VAS prediction average of 83% under random forest (**Supplementary Table 3**). Notably, Subject 2 consistently had the highest model accuracies across both binary and discrete VAS classification tasks. Feature importance was calculated by averaging the decrease in Gini Impurity for each feature of the random forest model, revealing that the total PIB values had the greatest contribution in model prediction among the feature types except for in Subject 4, where inter-channel correlations and coherences also had a higher percent contribution (see **Supplementary Figure S4**). It should be further noted that model prediction was lowest in both classification tasks for Subject 4.

Table 3. Multi-channel Binary VAS Prediction

Subject	Logistic Regression		Decision Tree		Random Forest		Linear Discriminant Analysis	
	Test	*Null*	*Test*	*Null*	*Test*	*Null*	*Test*	*Null*
1	66.7	49.4	72.8	54.3	81.5	49.4	58.0	50.6
2	94.6	48.6	96.4	43.2	100	52.2	100	55.9
3	77.4	47.6	70.2	47.0	80.4	49.4	56.0	48.8
4	70.3	64.9	63.1	58.6	75.7	64.9	61.3	49.5
5	68.9	52.2	69.4	54.4	77.2	48.3	56.7	45.0
Mean	75.6	52.5	74.4	51.5	83.0	52.8	66.4	50.0

Table 4. Multi-channel Discrete VAS Prediction

Subject	Logistic Regression		Decision Tree		Random Forest		Linear Discriminant Analysis	
	Test	*Null*	*Test*	*Null*	*Test*	*Null*	*Test*	*Null*
1	58.0	18.5	61.7	24.7	70.4	19.8	40.7	19.8
2	91.0	34.2	83.8	39.6	94.6	54.1	80.2	36.0
3	57.1	28.0	57.7	24.4	68.5	36.3	20.2	7.7
4	36.9	30.6	38.7	28.8	31.5	30.6	33.3	22.5
5	47.2	13.9	44.4	10.0	56.1	18.3	23.3	12.8
Mean	58.0	25.0	57.3	25.5	64.2	31.8	39.5	19.8

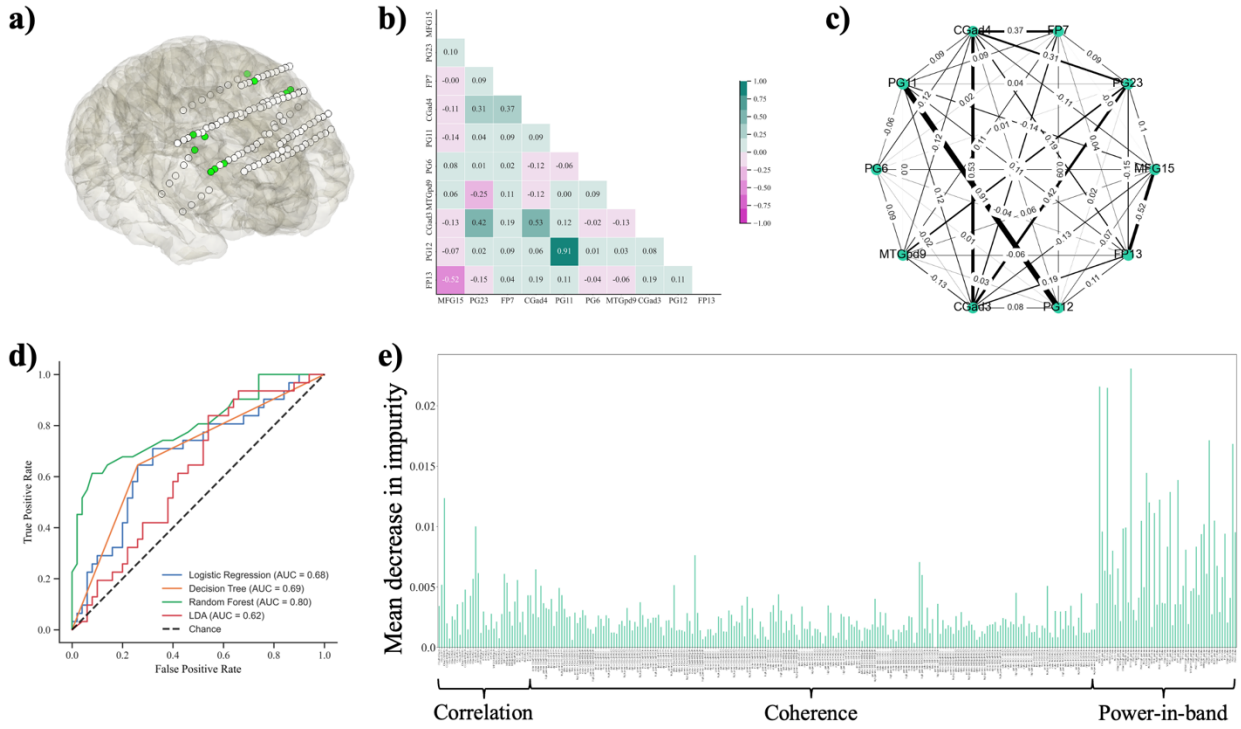

Fig. 5. Multi-channel pain prediction using correlation, coherence, and power-in-band values across pain reports. a) Pain network selection in Subject 1 using the top 10 best performing logistic regression models. b) Example feature calculations; Spearman's rank correlation coefficient computed for all combinations of channels in the pain network for a single pain report. c) Visual graph representation of the pain network for a single pain report with weight annotations equal to correlation values. d) Receiver-operator-curve comparing across model results for binary classification (low vs. high pain). e) Feature recruitment in the best performing full VAS classification model, random forest, as measured by mean decrease in Gini impurity.

Top-down Network Construction

Lastly, we constructed networks by evaluating Spearman's correlations between all channels, averaging across the low and high pain states. We calculated a difference matrix by subtracting the low pain state correlation matrix from the high pain state. We then applied a threshold to the difference matrix to create pain networks involving the channel connectivity values that varied the most.

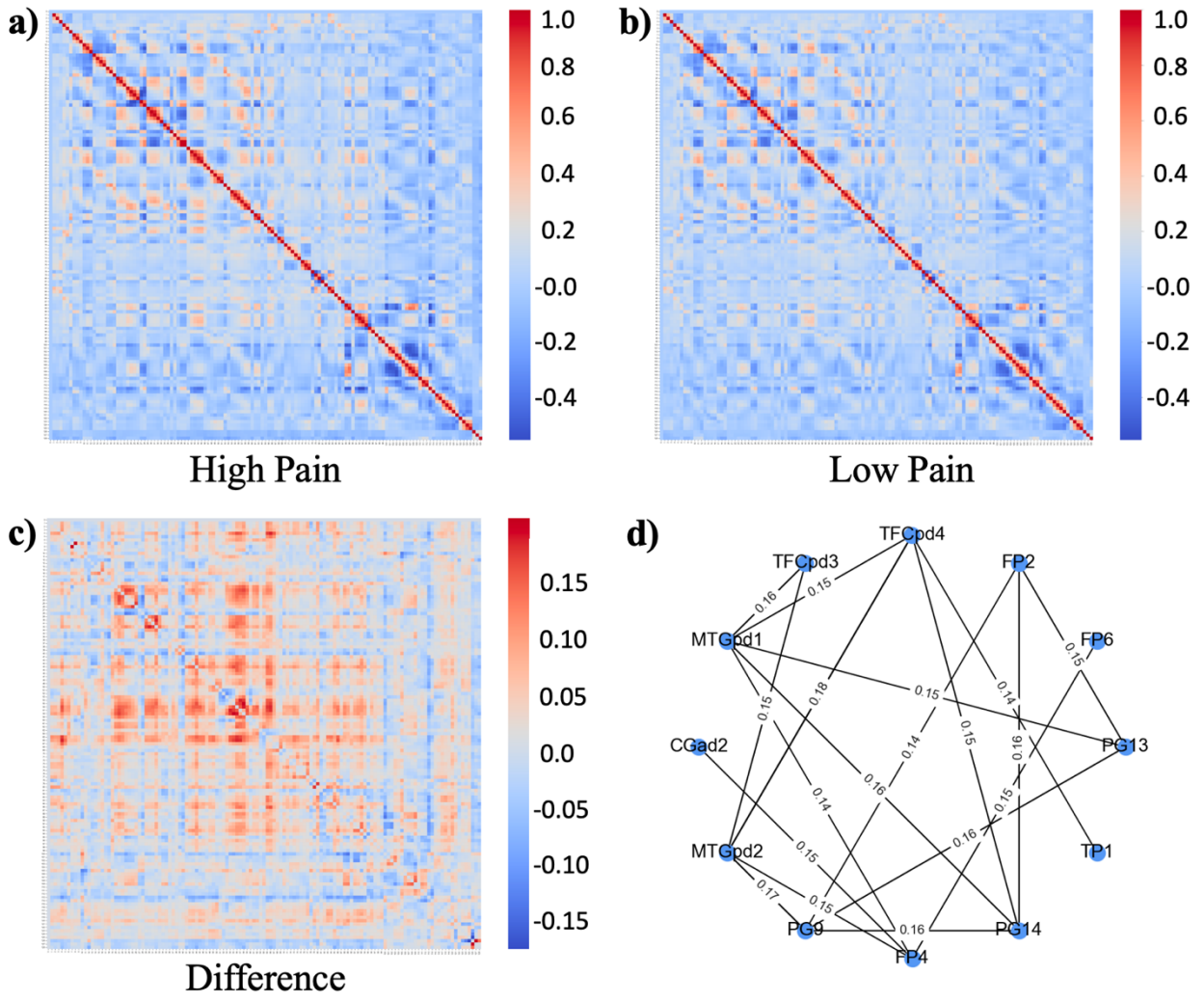

Fig. 6. Top-down network construction for Subject 1. a) Average cross-channel correlations for the high pain state. b) Average cross-correlations for the low pain state. c) Difference matrix between high and low pain state averages d) Graph representation of the difference connectivity matrix after thresholding to yield approximately 10 channels.

An example comparison between the bottom-up and top-down networks can be seen in **Figure 7**. For the bottom-up approach, we selected channels based on their individual performance in classifying low vs. high pain state from frequency features, whereas in this top-down approach, we measured an average connectivity map between the low vs. high pain state. Traditional connectivity methods utilize cross-correlations, but these can be computationally expensive when conducted on all possible channels. Our bottom-up approach builds off previously successful models to establish a pain network. Notably, both approaches draw from the precentral gyrus, middle temporal gyrus, frontal pole, and cingulate gyrus for Subject 1. Subjects 2, 3, and 5 also shared regions across the network construction types, with the middle temporal gyrus and precentral gyrus amongst common channels. In subjects 2, 3, 4, and 5, top-down networks relied heavily on local connections and single-site 'hubs', where one channel is correlated with many others (see **Supplementary Figure S7**). In Subject 4, all channels selected in the top-down network were from the left hippocampal tail, which was not included in the bottom-up network.

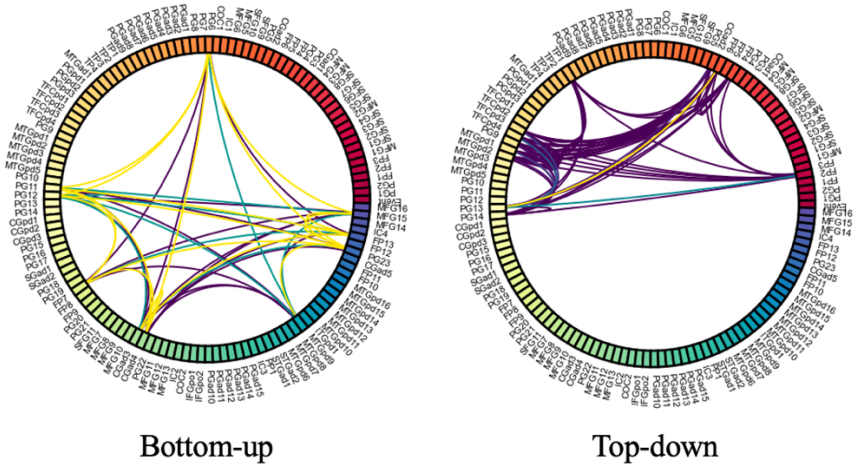

Fig. 7. Subject 1 comparison between bottom-up (using top 10 of the best performing channels in logistic regression) and top-down (using cross-correlations across all possible channels and applying a threshold).

DISCUSSION

We developed a machine learning paradigm to assess single-site, dual-site, and network-level models in predicting reported VAS scores (0–10) in humans (n=5). In binary pain classification, we demonstrated that single-channel logistic regression outperformed multi-channel logistic regression in in three out of five subjects. The best performing single-channel model was trained using beta band power of the inferior frontal gyrus in Subject 2 and had a classification accuracy of 99%. However, multi-channel random forest models outperformed single-channel logistic regression in decoding binary pain states in four out of five subjects. In discrete VAS prediction, we demonstrated that multi-channel models outperformed single channel models. In both binary and discrete VAS prediction, the multi-channel random forest model performed the best across subjects with mean accuracies of 80% for binary classification and 65% for discrete prediction. Feature importance for the random forest models using the Gini impurity measure revealed that the PIB values had a greater influence on model performance than channel pair correlations and coherences in four out of five subjects. These results indicate that (1) multi-channel PIB features outperform single-channel PIB features, likely due to it providing more information about pain responses across brain networks, and (2) PIB values are more predictive of pain fluctuations compared to connectivity measures such as correlation or coherence, which is surprising due to our prior understanding that pain networks interact to create the subjective experience of pain.

The best single-channel models were trained using PIB values from channels in the precentral gyrus (Subjects 1, 2, and 3), middle frontal gyrus (Subjects 1, 2, and 3) and inferior frontal gyrus (Subjects 2, 3, and 5). These regions and others from the frontal lobe that were included in our networks have been previously identified in neuroimaging studies [30]. Subject 4 had channel coverage that differed substantially from the other subjects. The channels in the best-performing models of Subject 4 were in pain structures including the anterior cingulate cortex and the emotion and memory regulating regions of the amygdala and hippocampus [31]. The occipital region appeared in Subjects 4 and 5, which is usually associated with visual processing and

perception, but has also been implicated in pain networks in rodents [32]. The best performing models across all subjects utilized PIB values from the beta band, gamma band, and high-gamma band. A notable region of interest occurred in the middle frontal gyrus of Subject 2, in which beta PIB values had high accuracy across several channels. The beta band in the middle frontal gyrus has been previously associated with the attention circuits of the brain [33]. Attention has been linked as a factor in increasing pain perception [34]. It is possible that the activation of the MFG in this subject corresponds to greater attention to their pain, indicated by the larger power-in-band values in the higher pain state compared to the lower pain state.

Subject 2 had the highest average prediction accuracy across subjects, and we hypothesize that this is attributable to the bimodal distribution of Subject 2's recorded VAS intensities. In Subject 2, half of the reported pain intensities were zero with the other half greater than zero, whereas other subjects had VAS scores that were more normally distributed, clustering around fours, fives, and sixes, as exemplified by Subject 4 (**Figure 1**). Since the median was drawn between a 0 and 1 VAS score for Subject 2, in binary tasks this meant classifying between a "yes" and "no" pain state. Controlling for subject-specific VAS distributions was not performed in this study but has been performed using a thermal grill illusion [35]. Future iterations of pain decoding may rely on additional measures such as the McGill Pain Questionnaire, which identifies sub-scores for both affective and sensory pain, previously associated with different neural structures [36]. Alternative approaches may account for pain medications or locations of pain.

The identification of these pain circuits can serve as reliable biomarkers for pain management strategies. Of particular interest are neuromodulation techniques which can directly affect signal transmission and has been used to treat subjects with chronic pain. The structures typically targeted in DBS for chronic pain relief are the thalamic ventral posterolateral and ventral posteromedial nuclei, periaqueductal gray matter, periventricular gray matter, posterior hypothalamus, nucleus accumbens, and anterior cingulate cortex [37]. In closed-loop deep brain stimulation, recordings from the regions of subject-specific pain circuitry may inform delivery and/or effectiveness of stimulation and enhance treatment efficacy [11].

There remain limitations to the study at present. First, the subject population is limited to patients with drug-resistant epilepsy who have invasive electrode implants for clinical monitoring purposes. Modeling brain activity from subjects with epilepsy may add confounds to neural electrophysiology because epilepsy is associated with changes in the electrical activity of the brain, mostly in the case of seizures [14]. In the current study, neural signals were analyzed and visualized to avoid overlap with epileptiform activity also known as ictal activity. However, it is unknown if these pain-related signals differ in subjects who do not have epilepsy. Currently, access to intracranial neural activity of subjects without epilepsy is limited. The main advantage of these datasets is the higher spatial and temporal resolution attained by iEEG, as opposed to non-invasive electroencephalography, occurring on the scalp.

Two different iEEG modalities were utilized for subject recording, sEEG and ECoG, based on clinical needs. While both iEEG modalities are biased toward the frontal and temporal lobes for subjects with epilepsy, ECoG is typically employed in cases where the laterality of the seizure onset zone is known and sEEG is typically used in cases where laterality is unknown [38]. The pain networks we identified in this study were limited by the type of electrode in addition to electrode placement. Our results did not indicate a difference between subjects with sEEG and ECoG recordings with respect to pain decoding. However, further expansion of population size

within both modalities is required to draw conclusions regarding whether the type of iEEG modality influences overall decoding performance.

A second limitation of the study is that since these subjects are undergoing seizure monitoring, the pain they report primarily consists of postoperative pain from the implantation of electrodes. Moreover, the subjects may be on anti-epileptic drugs and/or various pain medications, resulting in electrophysiology that may differ from everyday instances of pain such as from touching a hot stove or striking a finger with a hammer. In addition, the pain levels reported by the patients tended to decrease across their hospital stay. Our study at present takes the VAS scores at face value which may not reflect the variability in pain experiences in everyday life or across pain conditions.

The population size is another area for further investigation. Here we present data from five subjects, in which the pain-state decoding model is personalized to their neural activity. While some of our models recruited from pain structures previously implicated in the pain literature, applying these methods to additional subjects would allow for significance testing and further confirmation of pain-related neural electrophysiology. Due to differences in electrode coverage across subjects, group conclusions regarding pain networks would require significant overlaps in electrode placement, which may be possible with increased population size. Finally, there is an ongoing need for diverse subject populations, especially considering the uniqueness of an individual's pain experience.

REFERENCES

[1] R. Horn and J. Kramer, "Postoperative Pain Control," in *StatPearls*, Treasure Island (FL): StatPearls Publishing, 2023. Accessed: Jun. 09, 2023. [Online]. Available: http://www.ncbi.nlm.nih.gov/books/NBK544298/

[2] R. Kuner and T. Kuner, "Cellular Circuits in the Brain and Their Modulation in Acute and Chronic Pain," *Physiol. Rev.*, vol. 101, no. 1, pp. 213–258, Jan. 2021, doi: 10.1152/physrev.00040.2019.

[3] D. S. Goldberg and S. J. McGee, "Pain as a global public health priority," *BMC Public Health*, vol. 11, no. 1, p. 770, Oct. 2011, doi: 10.1186/1471-2458-11-770.

[4] "Global, regional, and national incidence, prevalence, and years lived with disability for 354 diseases and injuries for 195 countries and territories, 1990–2017: a systematic analysis for the Global Burden of Disease Study 2017 - The Lancet." https://www.thelancet.com/journals/lancet/article/PIIS0140-6736(18)32279-7/fulltext (accessed May 03, 2022).

[5] M. A. Lumley *et al.*, "Pain and Emotion: A Biopsychosocial Review of Recent Research," *J. Clin. Psychol.*, vol. 67, no. 9, pp. 942–968, Sep. 2011, doi: 10.1002/jclp.20816.

[6] K. E. Vowles, M. L. McEntee, P. S. Julnes, T. Frohe, J. P. Ney, and D. N. van der Goes, "Rates of opioid misuse, abuse, and addiction in chronic pain: a systematic review and data synthesis," *Pain*, vol. 156, no. 4, pp. 569–576, Apr. 2015, doi: 10.1097/01.j.pain.0000460357.01998.f1.

[7] "CDC Guideline for Prescribing Opioids for Chronic Pain — United States, 2016," *MMWR Recomm. Rep.*, vol. 65, 2016, doi: 10.15585/mmwr.rr6501e1er.

[8] K. Barrett and Y.-P. Chang, "Behavioral Interventions Targeting Chronic Pain, Depression, and Substance Use Disorder in Primary Care," *J. Nurs. Scholarsh.*, vol. 48, no. 4, pp. 345–353, 2016, doi: 10.1111/jnu.12213.

[9] R. G. Bittar *et al.*, "Deep brain stimulation for pain relief: a meta-analysis," *J. Clin. Neurosci. Off. J. Neurosurg. Soc. Australas.*, vol. 12, no. 5, pp. 515–519, Jun. 2005, doi: 10.1016/j.jocn.2004.10.005.

[10] M. Fana, G. Everett, T. Fagan, M. Mazzella, S. Zahedi, and J. M. Clements, "Procedural outcomes of deep brain stimulation (DBS) surgery in rural and urban patient population settings," *J. Clin. Neurosci.*, vol. 72, pp. 310–315, Feb. 2020, doi: 10.1016/j.jocn.2019.08.117.

[11] P. Shirvalkar, T. L. Veuthey, H. E. Dawes, and E. F. Chang, "Closed-Loop Deep Brain Stimulation for Refractory Chronic Pain," *Front. Comput. Neurosci.*, vol. 12, p. 18, 2018, doi: 10.3389/fncom.2018.00018.

[12] "Principles of Neural Science, 6e | AccessNeurology | McGraw Hill Medical." https://neurology.mhmedical.com/book.aspx?bookid=3024 (accessed Apr. 25, 2022).

[13] E. L. Garland, "Pain Processing in the Human Nervous System: A Selective Review of Nociceptive and Biobehavioral Pathways," *Prim. Care*, vol. 39, no. 3, pp. 561–571, Sep. 2012, doi: 10.1016/j.pop.2012.06.013.

[14] J. Scholz, "Mechanisms of chronic pain," *Mol. Pain*, vol. 10, no. Suppl 1, p. O15, Dec. 2014, doi: 10.1186/1744-8069-10-S1-O15.

[15] D. L. Morton, J. S. Sandhu, and A. K. Jones, "Brain imaging of pain: state of the art," *J. Pain Res.*, vol. 9, pp. 613–624, Sep. 2016, doi: 10.2147/JPR.S60433.

[16] B. Kulkarni *et al.*, “Attention to pain localization and unpleasantness discriminates the functions of the medial and lateral pain systems,” *Eur. J. Neurosci.*, vol. 21, no. 11, pp. 3133–3142, Jun. 2005, doi: 10.1111/j.1460-9568.2005.04098.x.
[17] Z. S. Chen, “Decoding pain from brain activity,” *J. Neural Eng.*, vol. 18, no. 5, Oct. 2021, doi: 10.1088/1741-2552/ac28d4.
[18] G. Buzsáki, C. A. Anastassiou, and C. Koch, “The origin of extracellular fields and currents — EEG, ECoG, LFP and spikes,” *Nat. Rev. Neurosci.*, vol. 13, no. 6, pp. 407–420, May 2012, doi: 10.1038/nrn3241.
[19] A. M. Bastos and J.-M. Schoffelen, “A Tutorial Review of Functional Connectivity Analysis Methods and Their Interpretational Pitfalls,” *Front. Syst. Neurosci.*, vol. 9, 2016, Accessed: May 08, 2023. [Online]. Available: https://www.frontiersin.org/articles/10.3389/fnsys.2015.00175
[20] M. D. Greicius, G. Srivastava, A. L. Reiss, and V. Menon, “Default-mode network activity distinguishes Alzheimer’s disease from healthy aging: evidence from functional MRI,” *Proc. Natl. Acad. Sci. U. S. A.*, vol. 101, no. 13, pp. 4637–4642, Mar. 2004, doi: 10.1073/pnas.0308627101.
[21] A. Anand *et al.*, “Activity and connectivity of brain mood regulating circuit in depression: a functional magnetic resonance study,” *Biol. Psychiatry*, vol. 57, no. 10, pp. 1079–1088, May 2005, doi: 10.1016/j.biopsych.2005.02.021.
[22] J. I. Tracy and G. E. Doucet, “Resting-state functional connectivity in epilepsy: growing relevance for clinical decision making,” *Curr. Opin. Neurol.*, vol. 28, no. 2, pp. 158–165, Apr. 2015, doi: 10.1097/WCO.0000000000000178.
[23] G. F. Stark *et al.*, “Using functional connectivity models to characterize relationships between working and episodic memory,” *Brain Behav.*, vol. 11, no. 8, p. e02105, Aug. 2021, doi: 10.1002/brb3.2105.
[24] K. Tran, B. H. Salazar, T. B. Boone, R. Khavari, and C. Karmonik, “Classification of multiple sclerosis women with voiding dysfunction using machine learning: Is functional connectivity or structural connectivity a better predictor?,” *BJUI Compass*, vol. 4, no. 3, pp. 277–284, May 2023, doi: 10.1002/bco2.217.
[25] T. D. Wager, L. Y. Atlas, M. A. Lindquist, M. Roy, C.-W. Woo, and E. Kross, “An fMRI-Based Neurologic Signature of Physical Pain,” *N. Engl. J. Med.*, vol. 368, no. 15, pp. 1388–1397, Apr. 2013, doi: 10.1056/NEJMoa1204471.
[26] S. L. Collins, R. A. Moore, and H. J. McQuay, “The visual analogue pain intensity scale: what is moderate pain in millimetres?,” *Pain*, vol. 72, no. 1–2, pp. 95–97, Aug. 1997, doi: 10.1016/s0304-3959(97)00005-5.
[27] F. Pedregosa *et al.*, “Scikit-learn: Machine Learning in Python,” *J. Mach. Learn. Res.*, vol. 12, no. 85, pp. 2825–2830, 2011.
[28] L. Breiman, *Classification and Regression Trees*. New York: Routledge, 2017. doi: 10.1201/9781315139470.
[29] E. K. Naeini *et al.*, “Pain Recognition With Electrocardiographic Features in Postoperative Patients: Method Validation Study,” *J. Med. Internet Res.*, vol. 23, no. 5, p. e25079, May 2021, doi: 10.2196/25079.
[30] J. Kong, M. L. Loggia, C. Zyloney, P. Tu, P. LaViolette, and R. L. Gollub, “Exploring the brain in pain: activations, deactivations and their relation,” *Pain*, vol. 148, no. 2, p. 257, Feb. 2010, doi: 10.1016/j.pain.2009.11.008.

[31] K. T. Martucci and S. C. Mackey, “Neuroimaging of Pain: Human Evidence and Clinical Relevance of Central Nervous System Processes and Modulation,” *Anesthesiology*, vol. 128, no. 6, pp. 1241–1254, Jun. 2018, doi: 10.1097/ALN.0000000000002137.
[32] J. Díaz-de-Terán *et al.*, “Occipital Nerve Stimulation for Pain Modulation in Drug-Resistant Chronic Cluster Headache,” *Brain Sci.*, vol. 11, no. 2, p. 236, Feb. 2021, doi: 10.3390/brainsci11020236.
[33] S. Japee, K. Holiday, M. D. Satyshur, I. Mukai, and L. G. Ungerleider, “A role of right middle frontal gyrus in reorienting of attention: a case study,” *Front. Syst. Neurosci.*, vol. 9, 2015, Accessed: Jun. 03, 2022. [Online]. Available: https://www.frontiersin.org/article/10.3389/fnsys.2015.00023
[34] G. Crombez, I. Viane, C. Eccleston, J. Devulder, and L. Goubert, “Attention to pain and fear of pain in patients with chronic pain,” *J. Behav. Med.*, vol. 36, no. 4, pp. 371–378, Aug. 2013, doi: 10.1007/s10865-012-9433-1.
[35] D. A. Shin and M. C. Chang, “A Review on Various Topics on the Thermal Grill Illusion,” *J. Clin. Med.*, vol. 10, no. 16, p. 3597, Aug. 2021, doi: 10.3390/jcm10163597.
[36] R. Melzack, “The short-form McGill Pain Questionnaire,” *Pain*, vol. 30, no. 2, pp. 191–197, Aug. 1987, doi: 10.1016/0304-3959(87)91074-8.
[37] “Deep Brain Stimulation for Chronic Pain - ClinicalKey.” https://www.clinicalkey.com/#!/content/playContent/1-s2.0-S1042368022000158?returnurl=https:%2F%2Flinkinghub.elsevier.com%2Fretrieve%2Fpii%2FS1042368022000158%3Fshowall%3Dtrue&referrer=https:%2F%2Fpubmed.ncbi.nlm.nih.gov%2F (accessed May 07, 2023).
[38] J. Parvizi and S. Kastner, “Human Intracranial EEG: Promises and Limitations,” *Nat. Neurosci.*, vol. 21, no. 4, pp. 474–483, Apr. 2018, doi: 10.1038/s41593-018-0108-2.
[39] D. Szucs and J. PA. Ioannidis, “Sample size evolution in neuroimaging research: An evaluation of highly-cited studies (1990–2012) and of latest practices (2017–2018) in high-impact journals,” *NeuroImage*, vol. 221, p. 117164, Nov. 2020, doi: 10.1016/j.neuroimage.2020.117164.

Supplementary Material

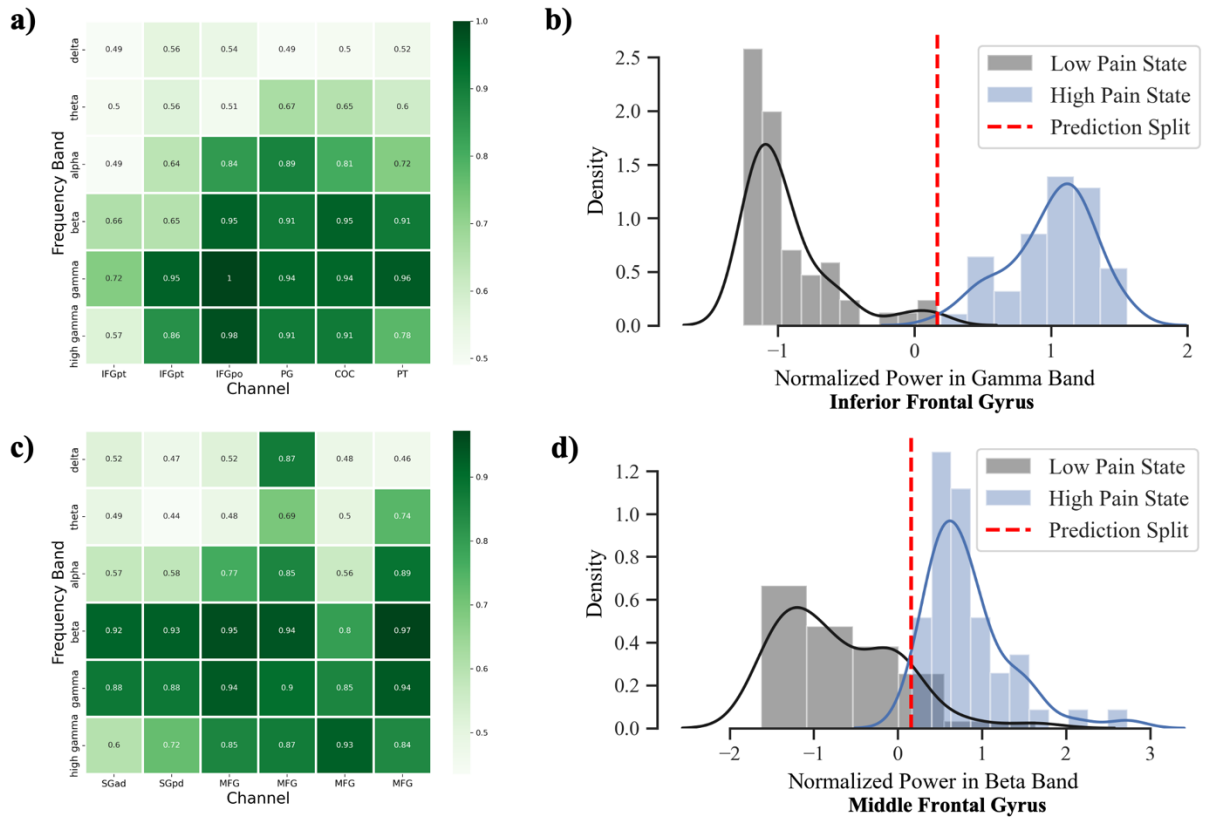

Fig. S1. Network selection by binary logistic regression search. Logistic regression models are trained on the normalized power-in-band for every combination of channel and frequency band. a, c) Network search shown in a region of 6 channels. b, d) Power-in-band values are computed across binary pain states.

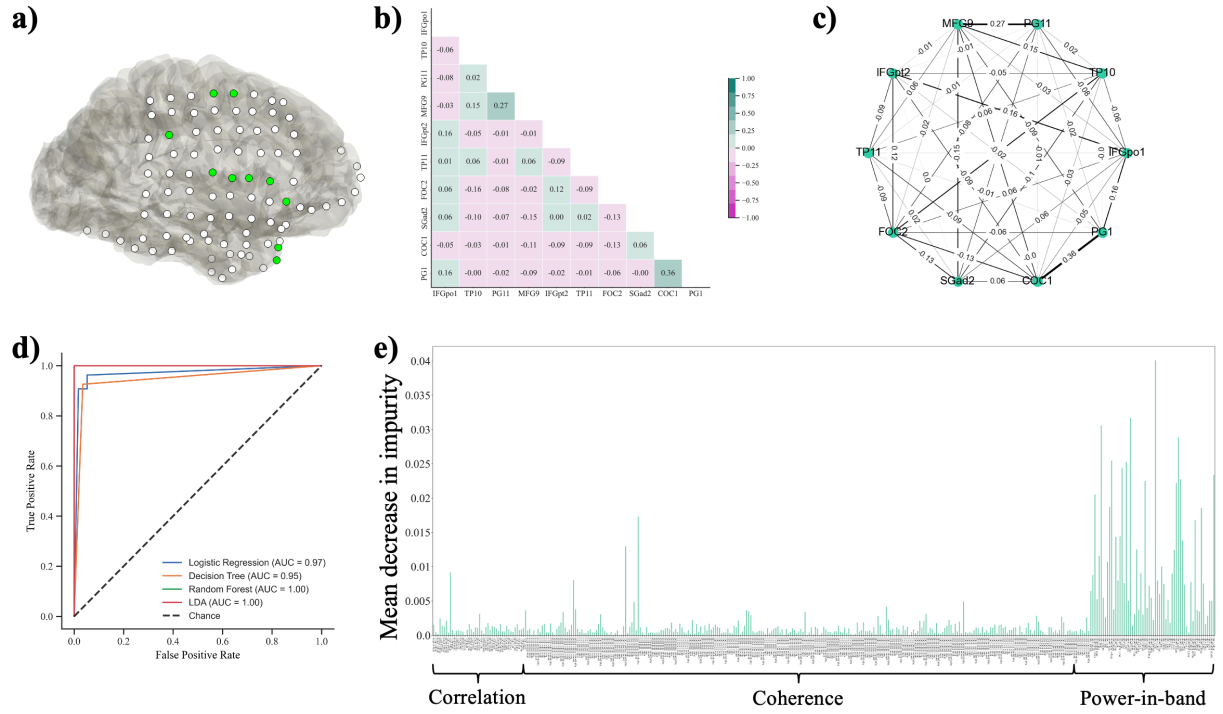

Fig. S2. Subject 2 network results. a) Pain network selection in Subject 2 using the top 10 best performing logistic regression models. b) Example feature calculations; Spearman's rank correlation coefficient computed for all combinations of channels in the pain network for a single pain report. c) Visual representation of the pain network for a single pain report. d) Receiver-operator-curve comparing results for binary classification (low vs. high pain). e) Feature recruitment in the best performing full VAS classification model, random forest, as measured by mean decrease in Gini impurity.

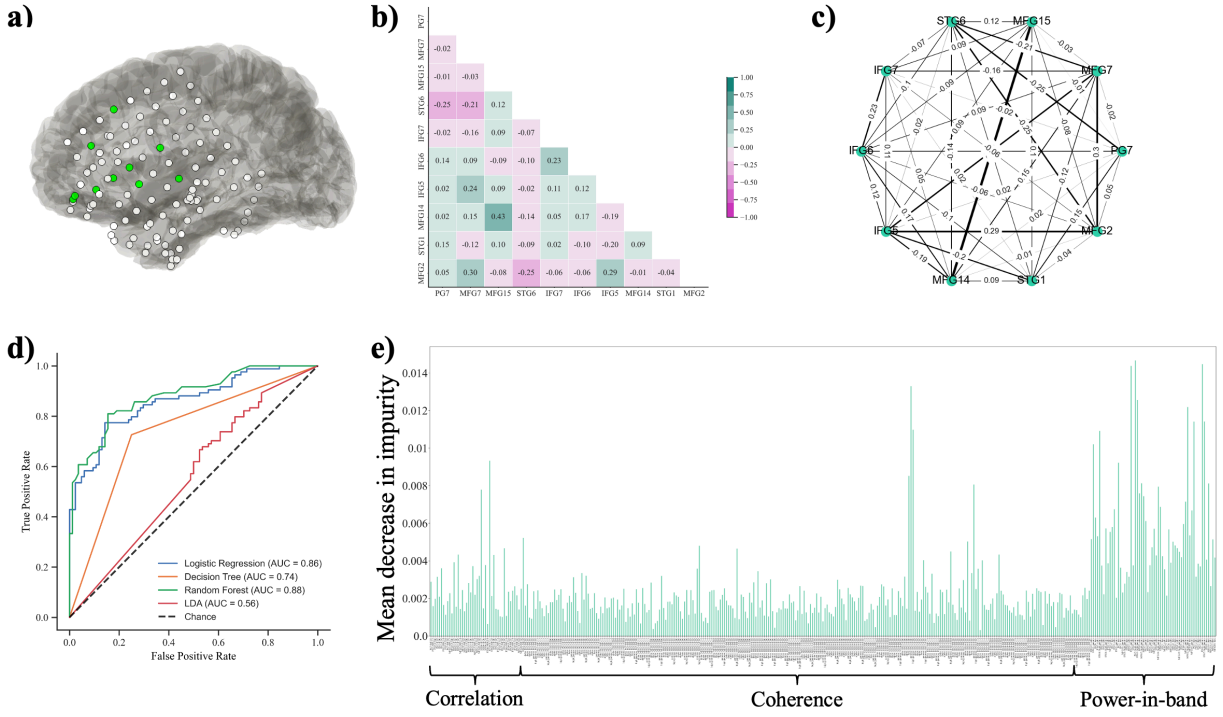

Fig S3. Subject 3 Network Results. a) Pain network selection in Subject 3 using the top 10 best performing logistic regression models. b) Example feature calculations; Spearman's rank correlation coefficient computed for all combinations of channels in the pain network for a single pain report. c) Visual representation of the pain network for a single pain report. d) Receiver-operator-curve comparing results for binary classification (low vs. high pain). e) Feature recruitment in the best performing full VAS classification model, random forest, as measured by mean decrease in Gini impurity.

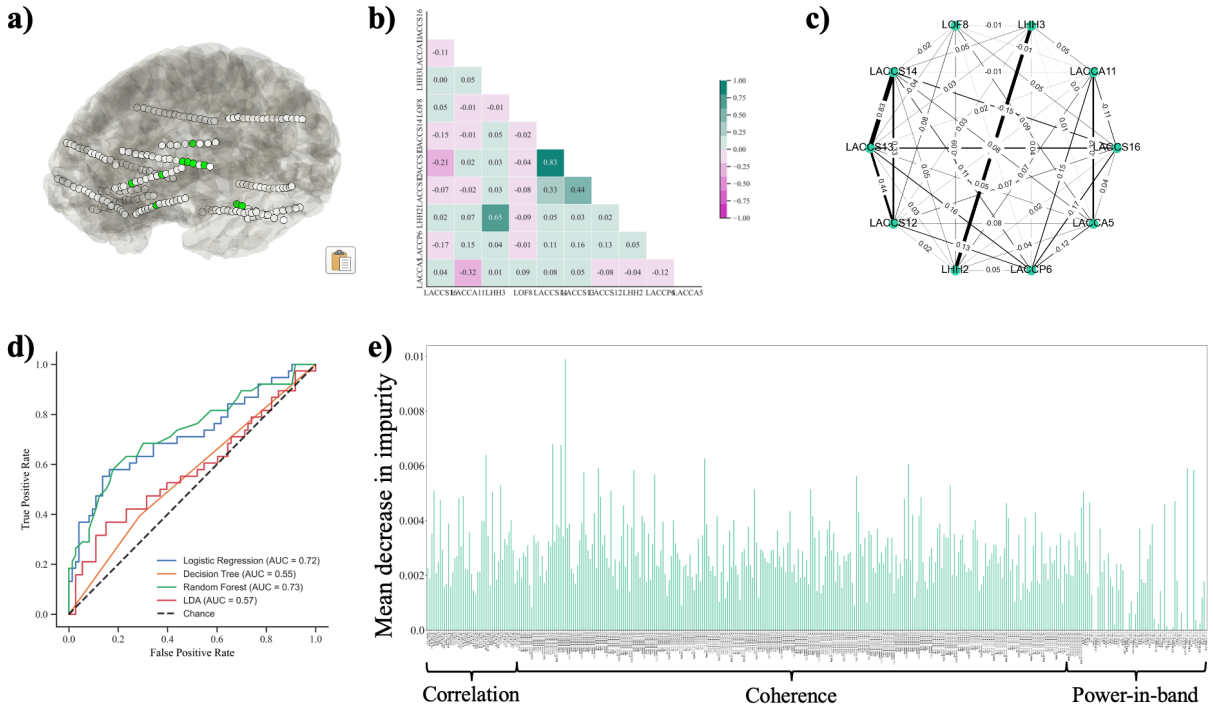

Fig S4. Subject 4 Network Results. a) Pain network selection in Subject 4 using the top 10 best performing logistic regression models. b) Example feature calculations; Spearman's rank correlation coefficient computed for all combinations of channels in the pain network for a single pain report. c) Visual representation of the pain network for a single pain report. d) Receiver-operator-curve comparing results for binary classification (low vs. high pain). e) Feature recruitment in the best performing full VAS classification model, random forest, as measured by mean decrease in Gini impurity.

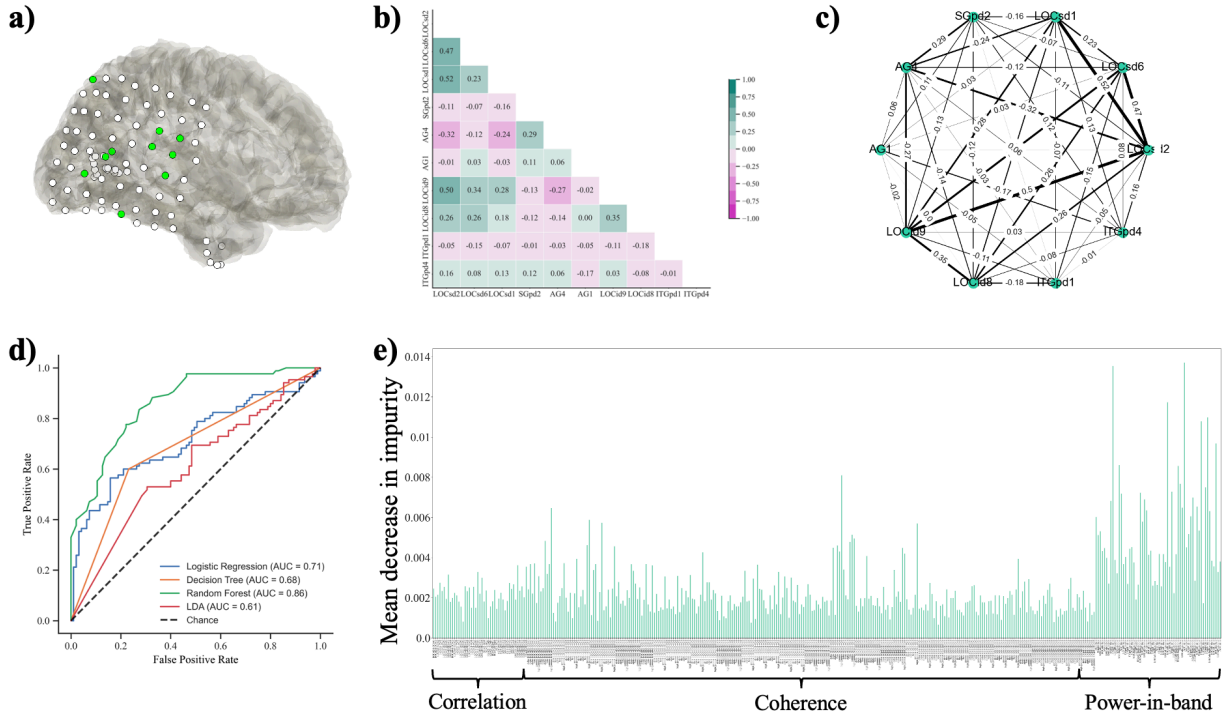

Fig S5. Subject 5 Network Results. Multi-channel pain prediction using correlation, coherence, and power-in-band values across pain reports. a) Pain network selection in Subject 5 using the top 10 best performing logistic regression models. b) Example feature calculations; Spearman's rank correlation coefficient computed for all combinations of channels in the pain network for a single pain report. c) Visual representation of the pain network for a single pain report. d) Receiver-operator-curve comparing results for binary classification (low vs. high pain). e) Feature recruitment in the best performing full VAS classification model, random forest, as measured by mean decrease in Gini impurity.

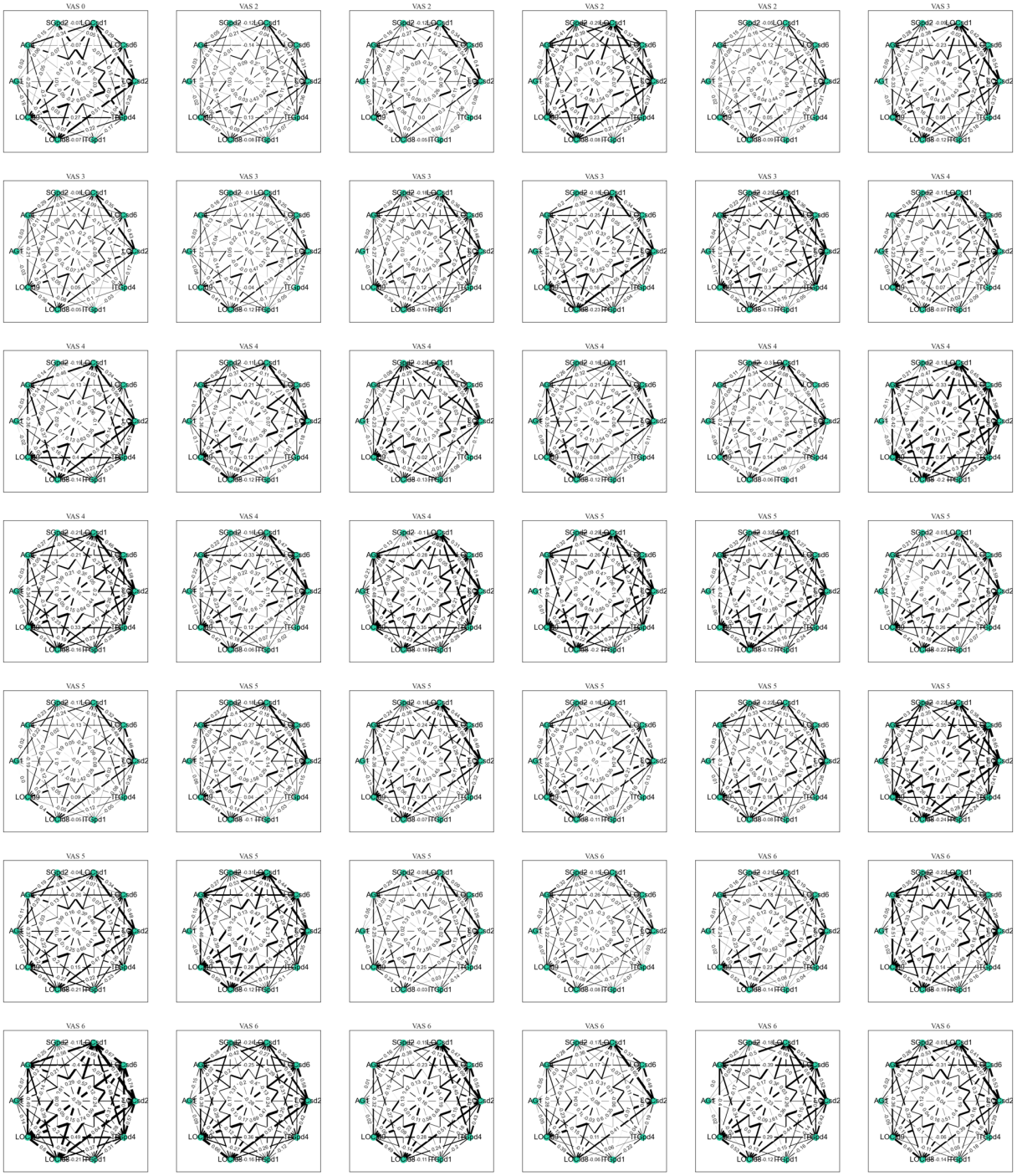

Fig S6. Exemplary networks across intensities. For each pain report, inter-channel calculations are computed. Our classifiers evaluate each instance of a network as a sample, compute features from that sample, and compare features across samples to predict the pain intensity of an unlabeled, test sample. Shown here are samples from Subject 5, values indicate Spearman's correlation coefficient.

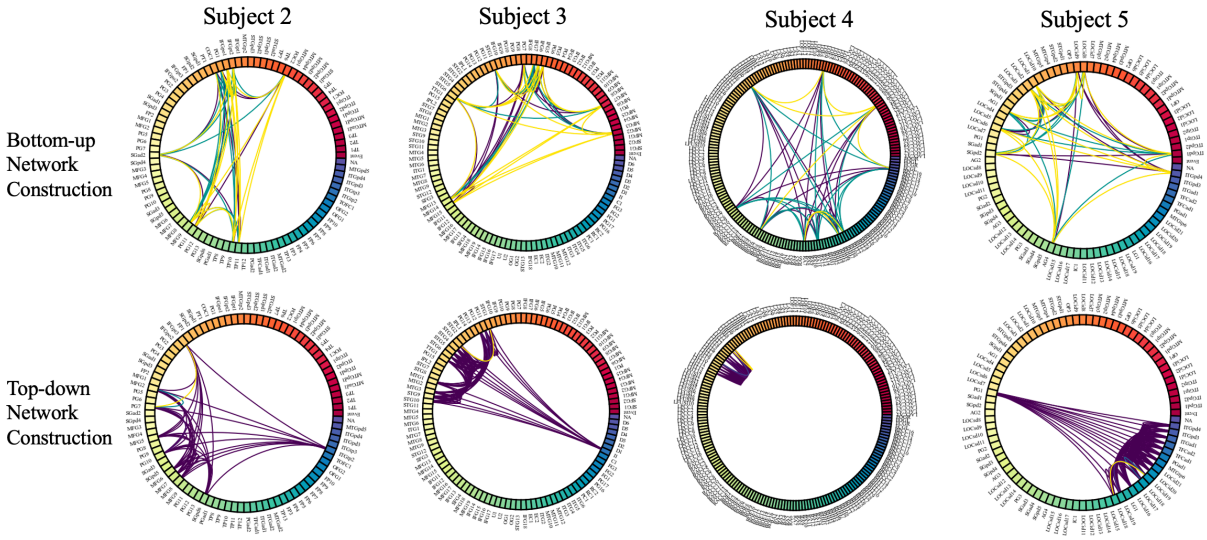

Fig S7. Network comparisons using the bottom-up approach (where channels are identified from the highest performing logistic regression models in the binary prediction task) and top-down approach (where channels are identified by applying a threshold to a difference matrix of Spearman's correlations between binarized low and high pain states.

Supplementary Table 1. Top-performing models for network selection

Subject	Region	Channel	Band	Logistic Regression Accuracy (%)
1	**Middle frontal gyrus**	**MFG15**	**high-gamma**	**74.1**
	Paracingulate gyrus	PG23	high-gamma	74.1
	Frontal pole	FP7	gamma	74.1
	Cingulate gyrus	CGad4	alpha	72.8
	Postcentral gyrus	PG11	high-gamma	72.8
	Precentral gyrus	PG6	high-gamma	72.8
	Middle temporal gyrus	MTGpd9	gamma	71.6
	Cingulate gyrus	CGad3	gamma	71.6
	Postcentral gyrus	PG12	beta	71.6
	Frontal pole	FP13	high-gamma	70.4
2	**Inferior frontal gyrus**	**IFGpo1**	**beta**	**99.1**
	Temporal pole	TP10	beta	97.3
	Precentral gyrus	PG11	gamma	97.3
	Middle frontal gyrus	MFG9	beta	97.3
	Inferior frontal gyrus	IFGpt2	gamma	97.3
	Temporal pole	TP11	beta	96.4
	Frontal orbital cortex	FOC2	beta	96.4
	Supramarginal gyrus	SGad2	beta	95.5
	Central opercular cortex	COC1	gamma	95.5
	Precentral gyrus	PG1	beta	95.5
3	**Precentral gyrus**	**PG7**	**beta**	**81.5**
	Middle frontal gyrus	MFG7	alpha	80.4
	Middle frontal gyrus	MFG15	theta	79.2
	Superior temporal gyrus	STG6	high-gamma	79.2
	Inferior frontal gyrus	IFG7	beta	79.2
	Inferior frontal gyrus	IFG6	theta	79.2
	Inferior frontal gyrus	IFG5	alpha	79.2
	Middle frontal gyrus	MFG14	theta	78.6
	Superior temporal gyrus	STG1	high-gamma	78.6
	Middle frontal gyrus	MFG2	gamma	78.6
4	**Hippocampus**	**RHH8**	**delta**	**77.5**
	Occipital frontal	ROF6	high-gamma	77.5
	Hippocampus	LHH6	gamma	77.5
	Posterior cingulate cortex	RPCC16	high-gamma	76.6

	Hippocampus	RHH6	delta	76.6
	Occipital frontal	LOF6	beta	76.6
	Amygdala	RA12	theta	75.7
	Amygdala	RA7	alpha	75.7
	Anterior cingulate cortex	RACC8	alpha	75.7
	Anterior cingulate cortex	LACCS6	gamma	75.7
5	**Occipital cortex**	**LOCsd2**	**high-gamma**	**68.3**
	Occipital cortex	LOCsd6	theta	67.8
	Occipital cortex	LOCsd1	beta	66.7
	Supramarginal gyrus	SGpd2	theta	66.1
	Angular gyrus	AG4	alpha	65.6
	Angular gyrus	AG1	theta	65.6
	Occipital cortex	LOCid9	theta	63.9
	Occipital cortex	LOCid8	gamma	63.3
	Inferior temporal gyrus	ITGpd1	theta	63.3
	Inferior temporal gyrus	ITGpd4	gamma	62.8

Supplementary Table 2. Top-performing models ranked by region across subjects

Region	Frequency
Middle frontal gyrus	6
Occipital cortex	5
Inferior frontal gyrus	5
Precentral gyrus	4
Hippocampus	3
Angular gyrus	2
Frontal pole	2
Anterior cingulate cortex	2
Occipital Frontal	2
Postcentral gyrus	2
Superior temporal gyrus	2
Cingulate gyrus	2
Supramarginal gyrus	2
Temporal pole	2
Inferior temporal gyrus	2
Amygdala	2
Paracingulate gyrus	1
Posterior cingulate cortex	1
Middle temporal gyrus	1
Frontal orbital cortex	1
Central opercular cortex	1

Supplementary Table 3. Multi-channel Discrete VAS Prediction (± 1)

Subject	Logistic Regression		Decision Tree		Random Forest		Linear Discriminant Analysis	
	Baseline	±1	Baseline	±1	Baseline	±1	Baseline	±1
1	68.0	58.0	61.7	63.0	70.4	70.4	40.7	44.4
2	91.0	92.8	83.8	86.5	94.6	97.3	80.2	85.6
3	57.1	82.1	57.7	80.4	68.5	87.5	20.2	38.1
4	36.9	85.6	38.7	75.7	31.5	89.2	33.3	76.6
5	47.2	71.7	44.4	63.9	56.1	68.9	23.3	45.6
Mean	58.0	78.0	57.3	73.9	64.2	82.6	39.5	58.1